



HAL
open science

Role of surface-tension additive in coating framing effect topography

Mathilde Delory, Blandine Chorein, Anne-Catherine Brulez, Loic Mees, N. Grosjean, Thomas Fiorani, Stephane Benayoun

► To cite this version:

Mathilde Delory, Blandine Chorein, Anne-Catherine Brulez, Loic Mees, N. Grosjean, et al.. Role of surface-tension additive in coating framing effect topography. *Colloids and Surfaces A: Physicochemical and Engineering Aspects*, 2023, 658, pp.130554. 10.1016/j.colsurfa.2022.130554 . hal-04056483

HAL Id: hal-04056483

<https://hal.science/hal-04056483>

Submitted on 3 Apr 2023

HAL is a multi-disciplinary open access archive for the deposit and dissemination of scientific research documents, whether they are published or not. The documents may come from teaching and research institutions in France or abroad, or from public or private research centers.

L'archive ouverte pluridisciplinaire **HAL**, est destinée au dépôt et à la diffusion de documents scientifiques de niveau recherche, publiés ou non, émanant des établissements d'enseignement et de recherche français ou étrangers, des laboratoires publics ou privés.

Role of surface-tension additive in coating framing effect topography

Mathilde Delory^{1,4,*}, Blandine Chorein², Anne-Catherine Brulez², Loïc Mees³,
Nathalie Grosjean³, Thomas Fiorani⁴, Stephane Benayoun¹

¹Univ Lyon, Ecole Centrale de Lyon, Laboratoire de Tribologie et Dynamique des Systèmes, UMR CNRS 5513, 36 avenue Guy de Collongue, 69134 Ecully Cedex, France

²ITECH Lyon, France

³Univ Lyon, Ecole Centrale de Lyon, Laboratoire de Mécanique des Fluides et d'Acoustique, UMR CNRS 5509, 69134 Ecully Cedex, France

⁴Faurecia Interior Systems, Méru, France

* Corresponding author : mathilde.delory@ec-lyon.fr (M. Delory).

Keywords: Coating, Framing effect, Fat-edge, Surface-tension additive, Surfactant, Film formation, Evaporation, Levelling, Surface-tension gradients, Marangoni effect, PTV

Abstract

Materials are often coated with liquid coatings for functional or aesthetic purposes. However, liquid coating deposition may result in surface irregularities in the final film due to substrate topography or physico-chemical or thermo-capillary phenomena. The surface defect of interest in this work is the framing effect, a surface defect at the edges of coated substrates. This study enables an in-depth understanding of capillary phenomena near substrate edges during coating and evaporation. A particle tracking velocimetry (PTV) technique highlights coating flows resulting from hydrostatic pressure and thermo-capillary phenomena such as vapour recoil and surface-tension gradients. This fluid mechanics technique was coupled with topographical measurements to study and quantify the influence of coating flows on framing effect dynamics. Framing effect topography do not rely on coating surface tension but on the presence of surface tension additive at film free surface and of their behaviours toward evaporation conditions.

1. Introduction

In various industrial applications, liquid coatings add technical functionalities or aesthetic properties to materials. A continuous, homogenous liquid film covering the entire surface is essential for fabricating materials with such properties. However, controlling the thickness distribution of liquid coating on a sharp-edged curve of the substrate is challenging. The coating industry [1–3] has been struggling for decades with a defect found on a sharp-edged curved substrate called the “framing effect”, also known as the “picture framing effect”, “fat-edge effect” or “border effect”. This defect consists of an excess coating at the outer corner of the substrate edge. Recent studies [4,5] have highlighted edge topography as a

driving force for framing effect formation occurring via capillary forces at the onset of film at the edge [4,6], as shown in Fig. 1.

The framing effect is not observed for all liquid coatings and is dependent on the composition and viscosity of the liquid coating. However, most coatings deposited via wet processes show a framing effect. Coatings are complex multi-component fluids that undergo compositional and rheological changes during their transition into the solid phase that may result in surface irregularities due to process conditions, environmental conditions, or coating characteristics. Liquid coatings undergo solvent evaporation to solidify, which leads to compositional changes generating local surface-tension gradients [1]. Additional surface-tension gradients arise from temperature gradients due to local endothermic evaporation [7]. Whether solutal or thermal, capillary flows such as lateral or convection movements can occur within the liquid coatings. The thermo-capillary flows commonly called the “Marangoni effect” [8] have been observed during coating film formation [9]. The rheology of coating formulation or surface additives influences the convective flows [7]. Several studies [7,10–14] highlighted the significant influence of surface additives in the evaporation process through mass transfer across a gas–liquid interphase. In certain conditions, a low concentration of surface additives can drastically reduce the mass transfer [10,13,14].

Recent studies [4,6,15] have investigated the role of physico-chemical or rheological properties on the framing effect using experimental or numerical approaches. Sommer et al. [6] observed that the surface tension of the coating, γ , influences framing effect topography, and the its width, height and slope are proportional to γ . The surface tension of the coating is considered a physico-chemical parameter to describe its chemical nature. Solvent evaporation close to an edge may generate surface-tension gradients, and thus far, no experimental studies investigating surface-tension gradients arising during film formation close to an edge have been reported. Numerical modelling of coating flows and the influence of surfactant are nevertheless found in the literature [16–19].

The framing effect is similar to some extent to levelling process. Levelling of coating films has been well studied [20–23] since Orchard’s pioneering theoretical study in 1962. The findings of his study revealed that the levelling process is a function of the film thickness, surface tension of the coating, dynamic viscosity of the coating, and initial ripple wavelength (such as brush marks). However, his equation applicable to non-volatile and Newtonian flow did not consider the rheology of evaporating non-Newtonian coatings and was later finalised, particularly by Overdiep et al. [24]. Wang et al. observed a low influence of surface additives on the levelling process, probably due to the high viscosities of the coatings [23].

This study investigates surface-tension gradients and discusses the relation between surface tension and framing effect topography studied previously [4,15]. An innovative particle tracking velocimetry (PTV) approach was developed to visualise coating flows upon film application and during film formation by incorporating fluorescent particles in the coating formulation. These experiments will facilitate an understanding of the role of surface tension of the coating in driving capillary flows. This study also explores the influence of surface-tension additive concentration on surface-tension gradients. The framing effect occurs close to an edge; therefore, the evaporation homogeneity at the edge and in the centre of the substrate was investigated.

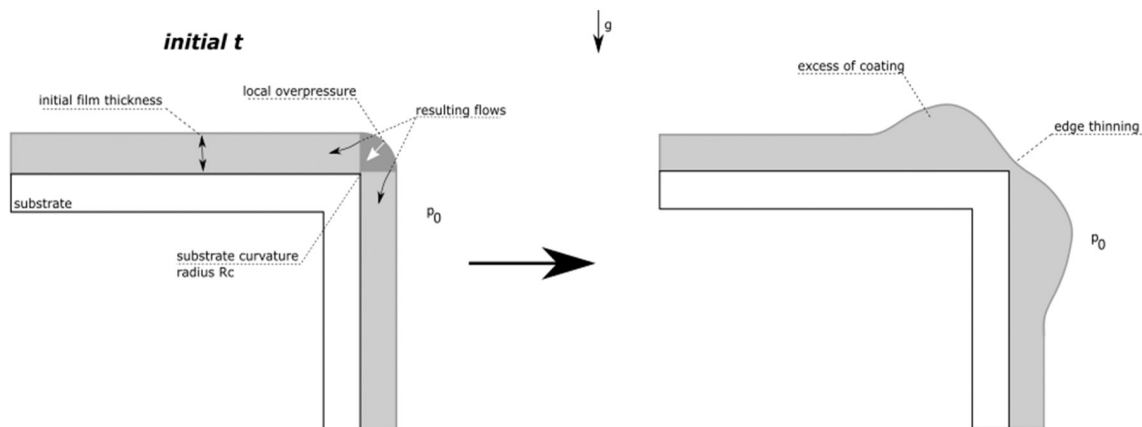


Fig. 1. Framing effect at a sharp-edged curved substrate.

2. Materials & methods

2.1. Materials

A two-component solvent-based polyurethane clear coat coating was used for the experiment. The formulations were prepared according to a model paint recipe provided by a coating supplier. The formulation was composed of an acrylic resin, aliphatic polyisocyanate hardener, solvents, and a surface-tension additive. A disperser operating at 1000 rpm was used to mix the weighed ingredients. The components of the solvent mix were carefully selected, considering the evaporation process and chemical compatibility with the other components. The primary solvent in the formulation was n-butyl acetate, a moderately volatile and versatile solvent. Other solvents in the formulation included xylene, light aromatic naphtha, and methoxy propyl acetate (PMA), whose physical properties are shown in Table 1. The solvent mix had a medium vaporization rate.

Table 1 : Physico-chemical data of solvents (from [25]).

| | CAS registry number | CE (coefficient of evaporation) | γ (mN/m) *experimental data |
|------------------------------|---------------------|---------------------------------|------------------------------------|
| n-butyl acetate | 123–86–4 | 1 (reference) | 25.3 * |
| Xylene | 1330–20–7 | 0.7 | 28.6 * |
| Light aromatic naphtha | 64742–95–6 | < 1 | 29.4 * |
| Methoxy Propyl Acetate (PMA) | 108–65–6 | 0.33 | 28.0 * |

Poly (methyl (alkyl) siloxane) formulated in xylene and purchased from company BYK was used as the surfactant. Poly (methyl (alkyl) siloxane) is chemically compatible with the formulation and can significantly reduce surface tension of coating. By incorporating surface tension additive in the coating formulation in varying quantities (0–1.7 wt%), coatings with different surface tensions were formed. The coating exhibited a dry extract of 62 ± 1.4 wt% and viscosity of 456 ± 28 mPa.s before coating application. The coating viscosity was measured using a Thermo Scientific MARS II rheometer involving a cone and plate geometry module (CP60). The surface tension of the final formulation was measured using a Wilhelmy balance technique using a Krüss K100 tensiometer, which varied with the amount of the surface- tension additive. In this study, the coating was seeded with fluorescent particles [Rhodamine B

doped (poly (methyl) methacrylate) (PMMA) microspheres, particle size distribution of 1–20 μm and specific gravity $\rho_p = 1.19 \text{ kg/m}^3$]. The excitation wavelength (λ) was 532 nm, and the fluorescent spectrum maximum was $\lambda = 580 \text{ nm}$.

Coating film applied with a hand coater under laser exposure had a final dry thickness of $54 \pm 18 \mu\text{m}$. Temperature and moisture were kept constant through the measurements. The substrates were $8 \times 4 \text{ cm}^2$ polycarbonate/acrylonitrile-butadiene-styrene (PC/ABS) injection moulded plaques with $0.087 \pm 0.02 \text{ mm}$ curvature radius. An injection mould was developed for this study to maintain control over the curvature radius and surface topography of the substrate ($R_a = 0.02 \mu\text{m}$). The surface energy of plastic substrates cleaned with isopropanol γ was measured along with its polar part γ_p and disperse part γ_d with Krüss DSA 30 tensiometer using the Owens, Wendt, Rabel and Kaelble (OWRK) method with water and diiodomethane as reference solvents ($\gamma = 48,7 \text{ mN/m}$, $\gamma_D = 48,3 \text{ mN/m}$, $\gamma_P = 0,9 \text{ mN/m}$).

2.2. Evaluation of evaporation rate

Gravimetric experiments were performed to evaluate the evaporation rate. Coating films were applied under similar conditions as those used during the PTV measurements to simulate the solvent evaporation process during PTV measurements. Immediately after coating deposition, the samples were weighed on a precision balance (accuracy of 0.0001 g) in a ventilated lab. Wet coating films of 150 μm thickness weighing $0.207 \pm 0.035 \text{ g}$ were deposited on the previously described injection moulded plastic substrate. The loss in weight due to evaporation was monitored as a function of time. The evaporation rate was calculated from the slope of the curve. A similar procedure was repeated three times for each sample.

2.3. Topographical characterization

Topographical characterization of framing effect on final coating film was performed using a single-point confocal chromatic profilometer (lateral resolution = 2.5 μm , height resolution = 0.1 μm , nominal measuring range = 1000 μm and reference = EVEREST-K1 optical pen from STIL). Topographical parameters of interest were: bump width w , height H , curvature c and maximal slope s , as defined in Fig. 2.

Dynamic monitoring of the topographical evolution was performed using a deflectometer until complete evaporation of the solvent. The specular property of the coated substrates enabled to monitor the evolution of bump curvature c and maximal slope s with deflectometry. Curvature topography is directly linked to the bump profile. Surface cartography was performed using the MountainsMap software [26].

2.4. Temperature measurements

The surface temperature of evaporating droplets was measured using an infrared camera (acquisition 100 Hz, Altair software). Coating droplets were deposited on an iso-propanol cleaned plastic substrate, and the temperature was recorded immediately after deposition. The surface temperature was recorded as temperature stabilised, and this procedure was repeated ten times for each coating formulation.

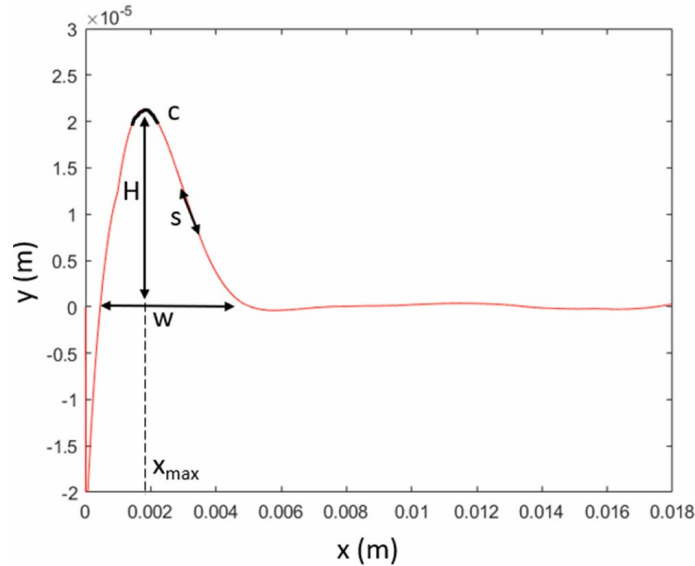


Fig. 2. Typical framing effect profile. Bump width w , height H , relative position x_{\max} , upper curvature c and maximal slope s .

2.5. Particle Tracking Velocimetry (PTV)

2.5.1. Experimental setup

PTV experimental setup shown in Fig. 3 was developed to perform 2D PTV measurements on freshly applied coating.

The acquisition system was composed of LaVision DaVis software (Version 10.1.1.60438), Navitar high-magnification zoom lens and pco edge sCMOS camera (resolution: 2560 × 2160-pixel, pixel size: 6.5 × 6.5 μm^2). Depending on experiments, the acquisition lasted for several minutes, with a frequency of 1 and 2 Hz (2 Hz was used when fast first movements were targeted). The lab-made optical system was composed of multiple lenses to obtain the thinnest laser sheet ($e < 0.4$ mm). A laser beam propagated through an optical arm to the optics. A diaphragm placed in front of the camera avoided any unnecessary luminosity. Optics and camera setup were installed on a micrometre platform to adjust the position of the laser sheet on the substrate and allow fine focusing. The Litron Bernoulli laser was used as a light source. Less than 5% of the maximum laser pulse energy (200 mJ per pulse) was used. The thin laser sheet was used to select one section of the flow. In addition, the limited depth of field (DOF) of the collection optic provided information on particle location, whose image was perfectly in focus in the centre of the laser sheet but slightly out of focus for particles near the edge of the illuminating beam, allowing the observation of displacements transverse to the visualisation plane.

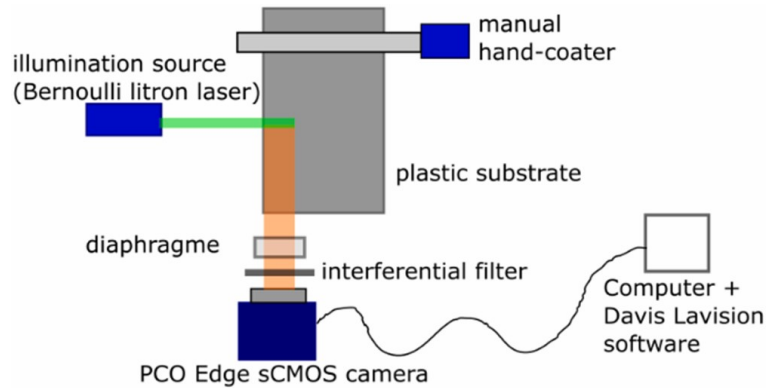


Fig. 3. Scheme for PTV experimental setup.

An interference filter (Edmund Optics, $\lambda = 591.5$ nm, 43 nm bandpass filter) was placed in front of the camera to select the fluorescent wavelength and discard the laser wavelength and noise associated with reflections on substrate and film interfaces. A typical video image is shown in Fig. 4.

Evaporation being an important factor in fluid flows, monitoring the local warm-up that the laser might induce is crucial. The optical system was calibrated using a commercial distortion test target from Edmund optics (0.125 μm diameter, 0.150 spacing) in ambient air. The framing effect is a defect on different scales, and it is 100 μm thick and several mm wide. However, an agreement was found between lateral and height information. The magnification ratio deduced from calibration was close to 2 (317.1 pixel/mm).

2.5.2. PTV post-treatment analysis

Image processing was done using the LaVision software. It consisted of image pre-processing (background subtraction), particle detection (on each image), and particle association from one image to another (particle tracking and vector displacement). Parameters for particle detection and particle tracking were optimised for the study. Approximately 30 particles per time step were detected and analysed. For a good correlation, the number of detected particles must be close to the number of active tracks with a minimum of lost tracks.

PTV post-treatment analysis was performed by converting particle tracks into the regular grid by Gaussian regression. A visualisation of the velocity vector map of fluorescent particles is proposed in Figs. 8, 9, 10. The film shape was added manually for better visualisation. Histograms representing the velocity distribution are also plotted: Every velocity vector representing the movement of a particle are sorted by its velocity v_x and counted.

2.6. Differences and agreement between measurement techniques

The various techniques used in this study operate at different scales and temporality. PTV is instantaneous and focuses on the initial 2 mm area close to the edge. In contrast, topographic measurement using deflectometry or profilometry has a broader measurement area (10–14 mm from the edge). The deflectometry is not an instantaneous technique because acquisition is made with the projection of multiple fringes that lasts 8 s; therefore, the result is not instantaneous but representative

of what happens during the acquisition process. The acquisition procedure makes the first measurement possible at 20 s after coating deposition.

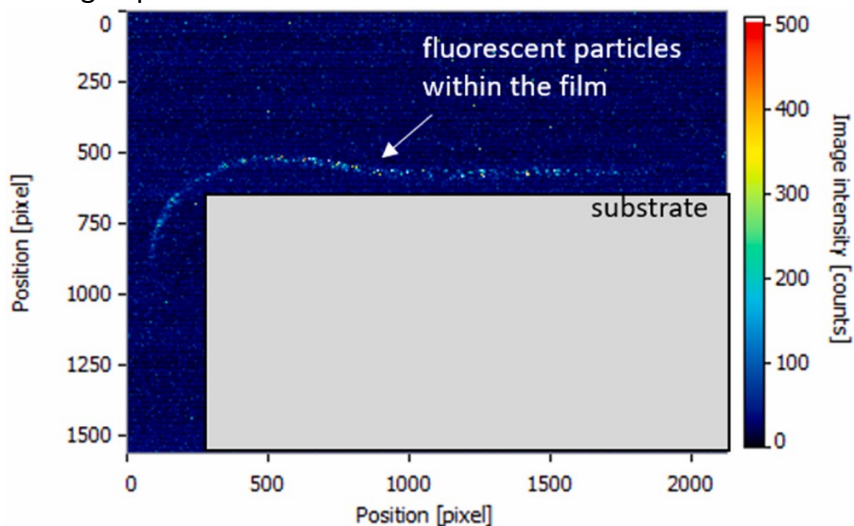


Fig. 4. Image recorded using PTV.

3. Results

3.1. Materials

Surface-tension additives added to a coating formulation reduce the surface tension of the coating [27]. Coating formulations with different surfactant concentrations were prepared, and the surface tension on every coating was measured using the Wilhelmy plate technique. Low surface-tension additive concentration significantly reduces the surface tension on the coating, and the profile flattens above 0.5% surface-tension additive concentration, as shown in Fig. 5.

3.2. Evaluation of evaporation rate

The influence of surface-tension additives on evaporation rate was evaluated using gravimetric analysis. By measuring the amount of material lost through the evaporation process on droplets having the same weight, different evaporation rates were observed for different surface-tension additive concentrations. The kinetic data for the evaporation rate generated from gravimetric analyses are shown in Table 2. Because the evaporation rate is evaluated on droplets and not films, a relative conclusion is considered rather than absolute values. Formulation without surface-tension additive exhibited an evaporation rate of $9.4 \cdot 10^{-4} \text{ w \% s}^{-1}$, whereas the formulation containing 0.3% surface-tension additive demonstrated an evaporation rate of $6.6 \cdot 10^{-4} \text{ w \% s}^{-1}$. Formulations with higher surface-tension additive concentrations indicated lower evaporation rates. The amount of surface-tension agent in the film directly impacts the evaporation rate.

For an in-depth analysis of the evaporation process, the surface temperature of evaporating droplets was measured with an infrared camera, and the results are reported in Table 3. Coating without surface-tension additive exhibited the lowest surface temperature of 19.8 °C, whereas coatings with 0.3% and 0.6% surface-tension additive had surface temperatures of 20.0 °C and 20.2 °C, respectively. Temperature

differences between ambient air temperature (reference) and the surface temperature of the film for different surfactant concentrations are shown in Table 3.

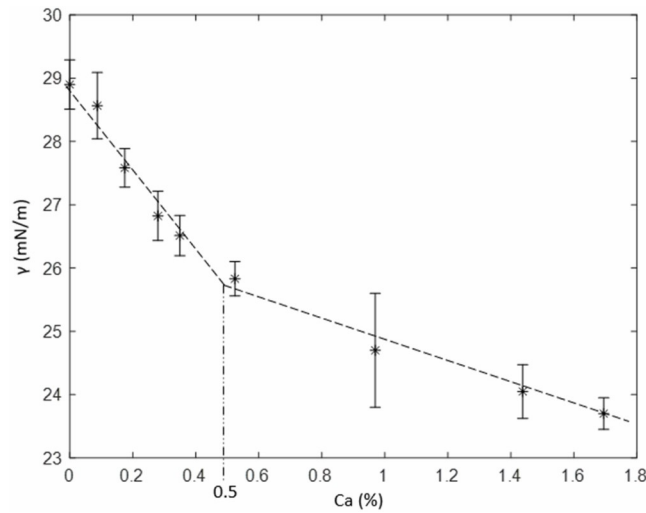


Fig. 5. Evolution of coating’s surface tension, γ , with surfactant concentration, Ca .

Table 2 Influence of surface-tension additive concentration, Ca , on evaporation rate, Ve .

| Ca (%) | 0 | 0.3 | 0.6 |
|--------------------------------|---------------|---------------|---------------|
| Ve ($10^{-4} w \% s^{-1}$) | 9.4 ± 2.2 | 6.6 ± 2.2 | 5.1 ± 3.5 |

Table 3 Influence of surface-tension additive concentration, Ca , on the temperature difference, ΔT .

| Ca (%) | 0 | 0.3 | 0.6 |
|-----------------|------|------|------|
| ΔT (°C) | 0.76 | 0.48 | 0.35 |

3.3. Topographical characterization

3.3.1. Influence of coating on the topography of the observed framing effect

Sommer et al. [6] determined the influence of surface tension on framing effect topography. This experimental study revealed similar results as Sommer et al. The topographical profiles of dried coating films show that high surface tension generates a narrower but steeper framing effect (border effect width is proportional to $1/\gamma$, and the slope is proportional to γ). Different coating formulations were applied on sharp-edged plastic substrates, and their framing effect was characterised. The influence of the coating’s surface tension on the topographical parameters of the framing effect is shown in Fig. 6. The surface-tension additive concentration influences different topographical parameters, bump height H and width w , maximal slope s and curvature c , as shown in Fig. 2. Slope and curvature increased for higher surface tension, whereas the width and relative maximum position decreased with surface tension. No significant variation was observed in the bump height.

Thus, formulations with higher surface tension have the steepest and highest framing effect, as depicted in Table 4.

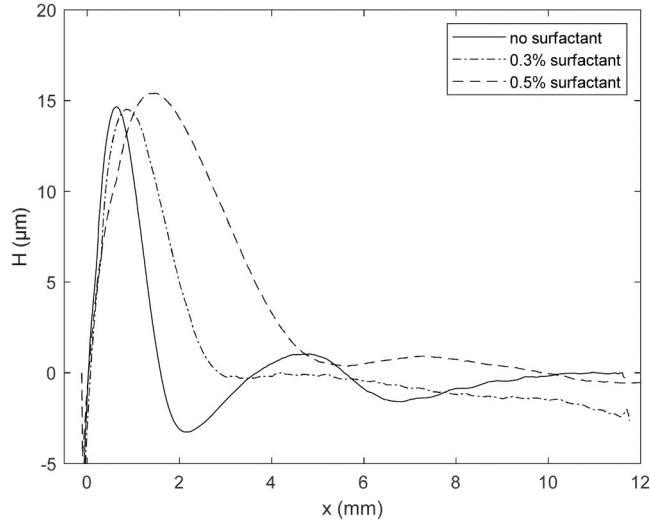


Fig. 6. Influence of coating surface tension on framing effect topography. H is the height of the framing effect and x the relative position.

Table 4 Influence of surface-tension additive concentration, Ca , on surface tension, γ , and topographic parameters (H its bump height, w its bump width, s its maximum bump slope).

| Ca (%) | 0 | 0.3 | 0.6 |
|---------------------------------|----------------|----------------|----------------|
| γ (mN/m) | 28.9 | 27.6 | 26.8 |
| H (μm) | 14.6 ± 4.3 | 13.2 ± 4.3 | 14.9 ± 4.7 |
| w (mm) | 2.6 ± 1.0 | 3.7 ± 0.7 | 5.8 ± 1.7 |
| s ($\mu\text{m}/\text{mm}$) | 10.5 ± 4.5 | 7.5 ± 1.0 | 5.0 ± 1.5 |

3.3.2. Kinetics of topographical evolution framing effect

Kinetic monitoring of topographical evolution using deflectometry provides some understanding of the previously described topography results. Formulation without a surface-tension additive was applied on a sharp-edged substrate. After 50 s of application, the framing effect shows one bump with its highest peak at $x = 1.6$ mm, as shown in Fig. 7 (a). This bump broadens during evaporation (curvature decreases), and its general morphology differs from the initial bump after 100 s of coating application. This broadening initiates the splitting of the initial bump; the bump separates into two different bumps at 200 s after application, as shown in Fig. 7(a). The first bump at $x = 0.7$ mm is the highest, with a curvature of 13.7 m^{-1} . The first bump is closer to the edge compared to the initial bump. Thus, the absence of a surface tension additive tends to bring materials to the edge as the framing effect splits the initial bump into two bumps.

In the case of a formulation with a 0.3% surface-tension additive, no such phenomenon was observed, as shown in Fig. 7(b). The curvature of the bump decreased from $c = 17.8 \text{ m}^{-1}$ to $c = 14.8 \text{ m}^{-1}$ and shifted from $x = 1.4$ mm to $x = 1.8$ mm. Kinetic data generated via deflectometry measurement shows that in the absence of surfactant, the bump is split, and part of the material is brought to the substrate edge, whereas with a 0.3% surface-tension additive bump retains the shape and is only slightly shifted ($\Delta x = 0.4$ mm) as the coating undergoes evaporation.

3.4. Particle Tracking Velocimetry

3.4.1. Coating temperature measurement through laser exposure

A PTV setup was developed to study the flow kinetics using deflectometry. An agreement between good image quality and a minimal local warm-up was achieved by adjusting the laser intensity. A local temperature increase of 0.08 °C was measured with an infrared camera. However, considering the limitation of acquisition frequency of the thermal camera, local temperature increase was neglected and was assumed not to modify the results.

3.4.2. Unilateral flow away from edges

PTV analysis enabled the visualisation of coating flows after application and during evaporation. All coating formulations (regardless of surface-tension additive concentration) experience a first horizontal material flow originating from the substrate edge towards the inner part of the substrate. PTV experiments allowed the quantification of speed for coating flows. A visualisation is proposed in Fig. 8(a), and a histogram for the distribution of coating flow speed through the film is plotted in Fig. 8(b). Depending on the particle considered and its position on the film, its speed and movement might differ; this explains the extensive distribution of speed values. Nevertheless, faster particles were found on the extreme edge, and exhibited speeds from 10 to 90 $\mu\text{m/s}$ as the flow spread right after coating application. This movement is initiated at the extreme substrate edge and propagates through the film.

3.4.3. Presence of vortical flows and lateral movement that brings material back to edges

After the first material flow, the second type of material flow appears for specific coating formulations ($\text{Ca} < 0.1\%$). Coatings without or with a low amount of surface-tension additive are affected. The onset of change in movement occurs between 40 and 60 s after application. As shown in Fig. 9, the film centre (around $x = 4.5 \text{ mm}$) is animated by the first flow propagation. In contrast, the film edge ($x = 2.0\text{--}3.7 \text{ mm}$) exhibits alternative movements; the onset of changes in material flow as particles shows some vorticity movements. During particle tracking, some particles indicate a first lateral movement of 0.1 mm either on the right or left, and then the same particle undergoes a second movement. The particle appears to go off the field, loses track for a while, and reappears. This movement is, however, not present within the depth of field. Vortical flows appearing for highly evaporating formulations could find their origin in the vapour recoil phenomenon. More data would be required to draw definitive conclusions, but following this line of thought, the departing vapour would provide an acceleration which exerts a reactive pressure on the interface, destabilizing the system locally [28,29].

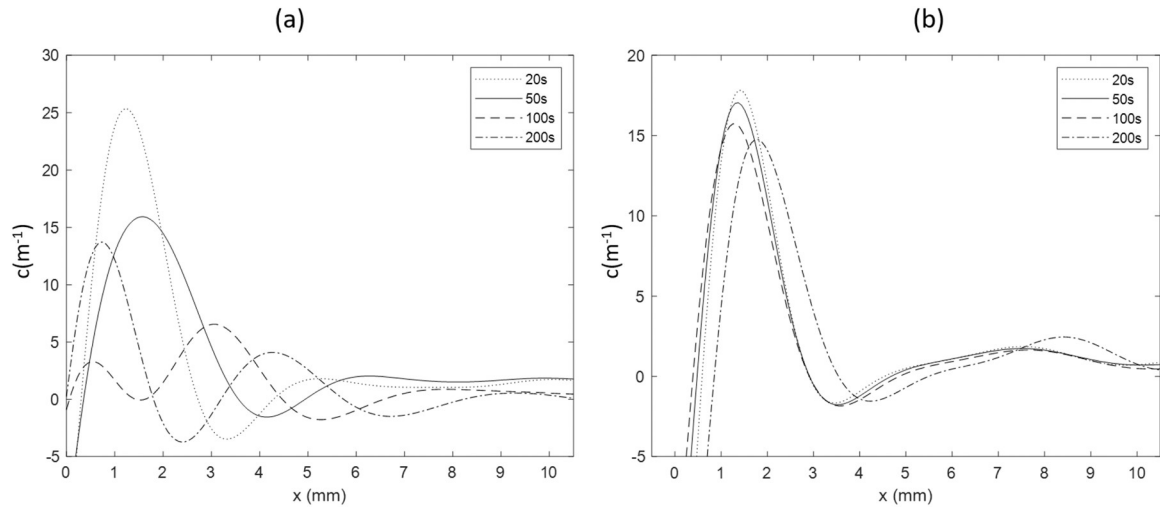


Fig. 7. Evolution of curvature, c , as a function of the relative position, x , during evaporation for formulations without surfactant, $Ca = 0\%$ (a) and with a surface-tension additive concentration, $Ca = 0.3\%$ (b).

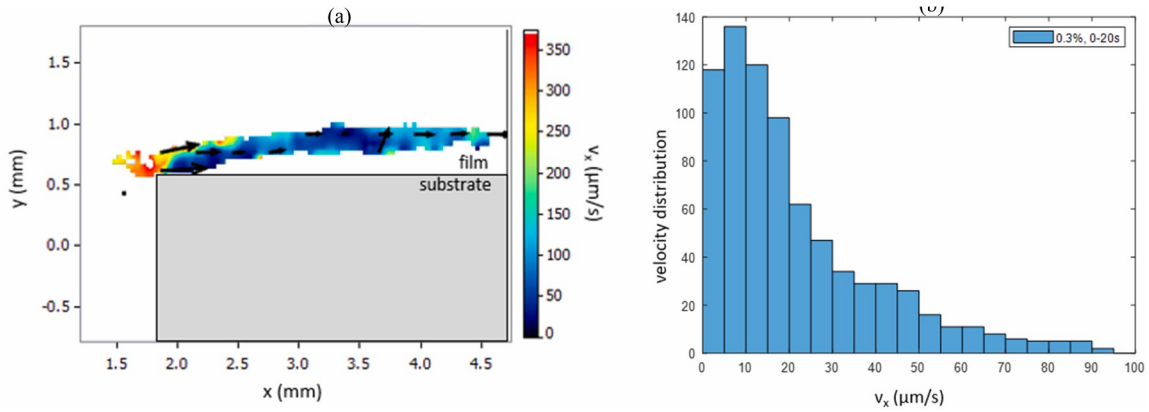


Fig. 8. Vector grid (a) and speed distribution (b) of coating flow (1–20 s experiment, surface-tension additive concentration, $Ca = 0.3\%$): spreading phase.

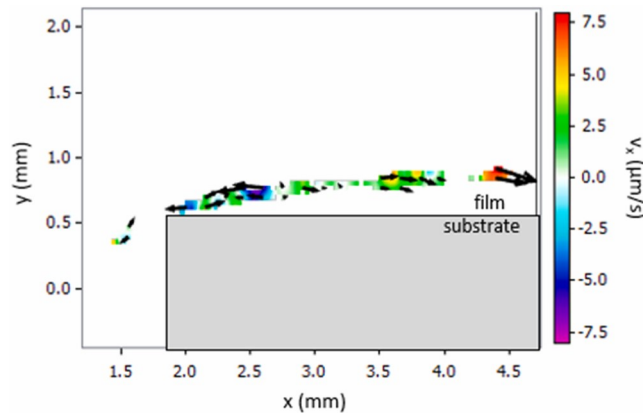


Fig. 9. Vector grid of coating flow (40–60 s experiment, surface-tension additive concentration, $Ca = 0\%$): onset of movement change.

The second coating flow occurs between 80 and 100 s after application; coatings without or with low surface-tension additive exhibit vortical flows and a movement towards the substrate edge. Vortical flows are parallel to substrate direction and are more prominent at the edge than on the film. Fig. 10 (a) depicts flow vectors pointing in both directions, most of them and the faster ones pointing towards the substrate edge. Fig. 10 (b) shows the speed distribution across the films and that particles move in both directions, but most move towards the edges. The movement of vortical or lateral flows was slower than the initial spreading movement induced by hydrostatic pressure.

4. Discussions

4.1. Role of surface tension on framing effect topography: a comparative study

The main objective of this study was to determine the influence of surface tension additive on framing effect topography. Few results on the influence of surface tension on framing effect topography can be found in the literature [5,15]. A comparison of topographical parameters of framing effects from different studies is plotted in Fig. 11(a) and 11(b) (Sommer et al. [5], Lee et al. [15] and this work). The three studies present alternative methods to evaluate the influence of surface tension of coating on the framing effect:

- Experimental study by Sommer et al. [5] (vertical coating)
- Experimental study in this work (manual horizontal coating)
- Numerical study by Lee et al. [15](Table 5)

The numerical study by Lee et al. does not depict a strong influence of surface tension on framing effect topography compared to the two other studies. Decreasing surface tension highly decreases bump height (data at $\gamma = 22$ mN/m), as shown by Sommer et al. However, this is not the case in this work as the surface tension operating window is smaller. These disagreements can be attributed to the use of different methods such as experimental or numerical, the method of coating application such as horizontal or vertical, and the differences in the coating composition (components and quantities), viscosity and substrate edge topography.

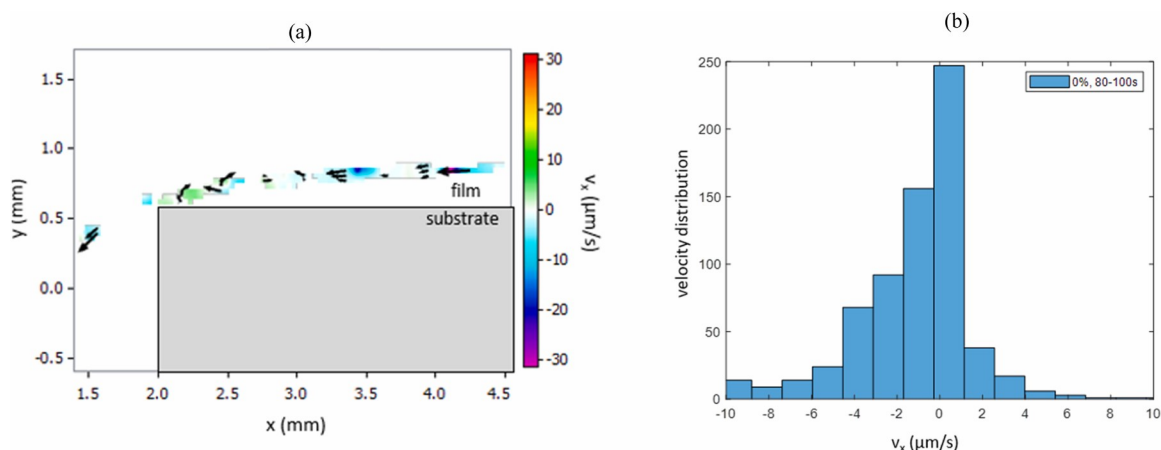


Fig. 10. Vector grid (a) and speed distribution (b) of coating flow (80–100 s experiment, surface-tension additive concentration, $Ca = 0\%$): vorticity flows that brings materials back to edge.

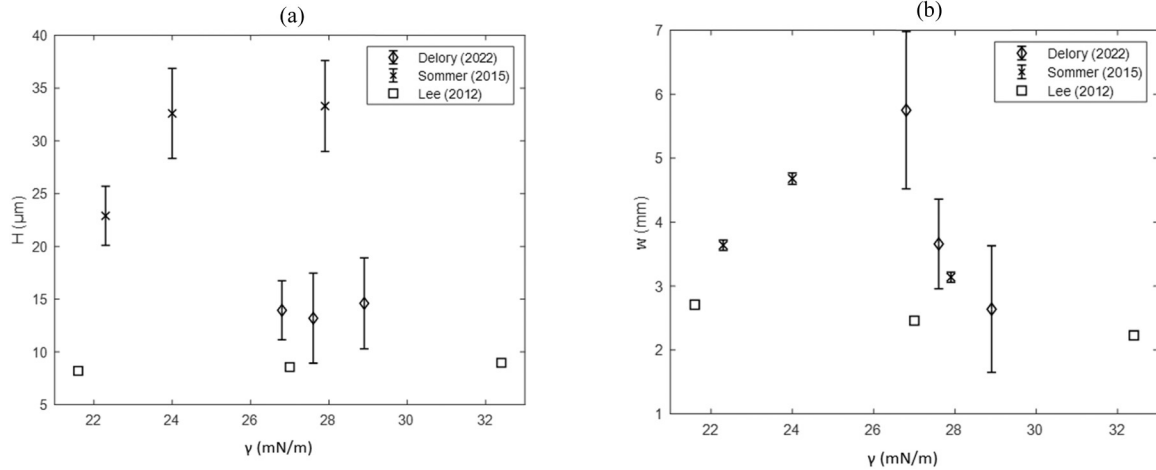


Fig. 11. Comparison of bump height, H , (a) and width (b) as a function of coating's surface tension, γ , from different studies.

Table 5 Comparison between the different methods found in the literature.

| | Sommer et al. [5] | Delory et al. | Lee et al. [15] |
|---------------------------------|-------------------|---------------|-----------------|
| Method | experimental | experimental | numerical |
| Substrate curvature radius (mm) | 0.1 | 0.1 | 0.3 |
| Substrate position | vertical | horizontal | horizontal |
| Viscosity η (kg/m.s) | 0.24 | 0.29 | 0.024 |

4.2. Role of surface tension additives in evaporation of coating

As previously mentioned, the surface tension of coating is modified by incorporating a surface-tension additive into the coating formulation. These surface-tension additives molecules can move primarily to the free film surface [27]. When the surface-tension additive concentration is near the critical micelle concentration (CMC), the free film surface is saturated, and above CMC, the surface-tension additive remains in the bulk of the film in the form of micelles. The surface tension of formulations with different amounts of the surface-tension additive was measured using the Wilhelmy method, as shown in Fig. 5 CMC was determined when surface tension remained steady with surface-tension additive concentration. Experimental results showed that CMC was around 0.5%. Fig. 12 schematises the repartition of surface-tension additive molecules depending on how relative surface-tension additive concentration is to CMC.

The coating formulation that exhibits the highest evaporation rate is the formulation without surface-tension additives as measured by gravimetric analyses and surface temperature, as shown in Tables 2 and 3. This interpretation has been reported in other studies [10,11,14]. In some conditions, the presence of surface-tension additives drastically reduce the mass transfer of solvent molecules through air-liquid interphase, slowing the evaporation. There is, however, an unanswered question: Is it the surface tension of coating, or is it the presence of surface-tension additives at the free film surface that drives this mechanism? Some insight into this question is provided because the evaporation rate is not proportional to the surface tension or the surface-tension additive concentration. A minimal amount of surface-tension additive in the formulation is enough to modify the evaporation of the whole coating droplet or film, and

beyond a given quantity of surface-tension additive, no more effect is observed on evaporation. These behaviours could be due to the surface-tension additive at the free film surface, affecting the mass transfer of solvent molecules through air-coating interphase [10,11,14] and hence, slowing down the evaporation process.

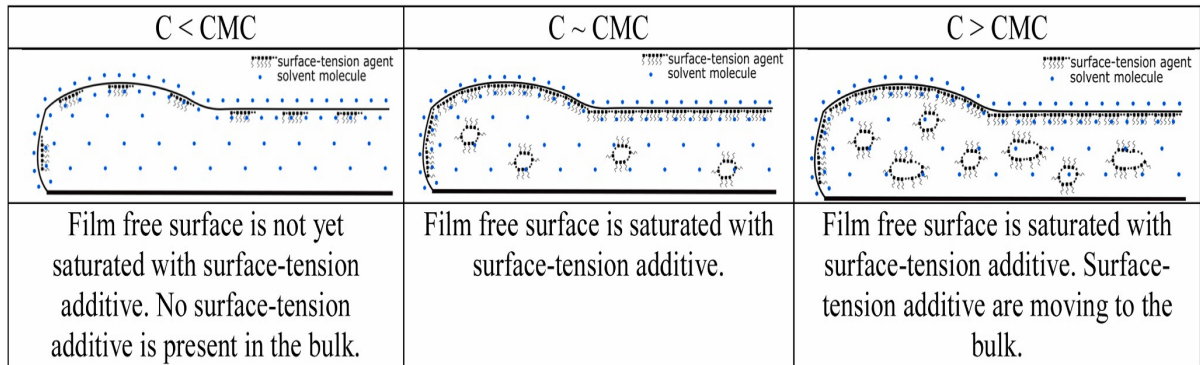


Fig. 12. Repartition of surface-tension additive in coating film in regard to surface-tension additive concentration’.

4.3. Role of surface tension additives in framing effect dynamics

As shown previously, modifying the surface tension of coating drastically affects framing effect topography. It is therefore essential to focus on framing effect dynamics depending on the surface tension of the coating. PTV observations highlighted different material flows in the coating film during film application and solvent evaporation, as shown by the scheme in Fig. 13. The surface tension of coating triggers different flows that can be, in some conditions, consecutive to one another. These results must be considered with the measurement area 2–2.5 mm close to the substrate edge.

- For all coating formulations, a first spreading phase occurs after coating application. This flow is the result of hydrostatic pressure initiated by the substrate edge, as highlighted by Sommer et al. [6]
- At low surface tension ($\gamma=26$ mN/m), that is, at a high surface-tension additive concentration ($Ca>0.3\%$), the only movement observed is the spreading phase, the coating being spread from the substrate edge through the film. There is a competition between spreading phenomena and viscous forces.
- At intermediate surface tension ($\gamma=27$ mN/m), that is, at a medium of surface-tension additive concentration ($0.1\%<Ca<0.2\%$), few vortical flows appear randomly around the edges after the spreading phase.
- At high surface tension ($\gamma=28$ mN/m) and in the absence of a surface-tension additive a significant number of vortical flows appear randomly around the edges after the spreading phase and are followed by a horizontal movement towards the substrate edge.

No convection flow was observed in the entire film thickness as described by Saranjam et al. [9] or Abbasian et al. [7] for the experimental conditions in this study. The Marangoni adimensional number defined by Zhang et al. [30] was calculated for the different surface tension of coatings and shown in

Table 6. Surface tension additive is added in a small concentration (Ca<0.5%) and is primarily present on the film surface; therefore, it does not affect the bulk physical properties of the coating. Hence, the data for calculating both formulations are $\rho = 1172 \text{ kg/m}^3$, $\mu = 460 \text{ mPa.s}$, $\Delta H = 60 \text{ J/g}$, $C_p = 1.9 \text{ J/gK}$ and $L = 100 \text{ }\mu\text{m}$. The calculation resulted in a low Marangoni number for all coatings ($Ma < 0.3$), suggesting a low probability of Marangoni convection occurring under these experimental conditions. Coatings with higher surface tension have a slightly higher Marangoni number than coatings with low surface tension (+32%).

Table 6 Marangoni adimensional numbers for coating formulations.

| | | |
|--|------|-------|
| Surface tension (mN/m) | 28.9 | 26.8 |
| Surface-tension additive (%) | 0 | 0.3 |
| ΔT (°C) | 0.76 | 0.48 |
| Evaporation rate (w\% s^{-1}) | 0.94 | 0.66 |
| Marangoni number (convection) | 0.29 | 0.195 |
| Marangoni number (evaporation) | 0.01 | 0.007 |
| Marangoni number Ma^* | 0.30 | 0.20 |

Equation 1: Marangoni adimensional number

$$Ma^* = \underbrace{\frac{\partial \gamma L c \cdot \Delta T}{\partial T \mu \cdot \alpha}}_{\text{convection}} + \underbrace{\frac{\partial \gamma \dot{V} \Delta h_v d^2}{\partial T \mu C_p \cdot \alpha^2}}_{\text{evaporation}}$$

Deflectometry measurements enabled a more comprehensive study of framing effect dynamics with its high measurement area. Different framing effect dynamics were highlighted based on the surface tension agent concentration. A first bump was generated at 20 s after coating application due to Laplace hydrostatic pressure. PTV analysis shows that this spreading phase stopped in the first 2 mm area close to the substrate edge (PTV measurement window) at 40–60 s after coating application, as shown in Fig. 9; however, spreading continued afterwards, as shown by deflectometry measurement for a 0.3 wt% surface agent formulation. Formulation with no surfactant depicted an initial bump split into two bumps after 100 s. A part of the coating material was pushed towards the substrate edge, as shown by PTV analysis at 80–100 s after coating application, and a second part of the coating material was pushed towards the film centre. A formulation with a 0.3 wt% surfactant did not show any of these movements; therefore, we hypothesised that these flows do not come from the continuation of spreading flow due to hydrostatic pressure. The split movement can be explained based on the levelling process of evaporating coating. However, the PTV measurement window could not analyse this entire movement. Overdiep et al. [24] investigated the effect of surface-tension gradients. The initial bump had a higher solvent concentration due to its excess material than the surrounding coating film. As the solvent had a lower surface tension than the resin, the areas with higher solvent concentration had a lower surface tension than those with lower solvent concentration. This would result in a movement from the bump to the surroundings according to the levelling theory [20,24]: the peak becomes a valley, and the valley transforms into two peaks. The presence of substrate edge nearby would block coating from further movements. As film mobility is the key to any material flow within the film, there might be a limit upon which no more movement is possible. To conclude, formulation with no surface agent depicts a competition between the

spreading phase and lateral surface-tension gradients. The 200 s-curvature profile shows that flows initiated by lateral surface-tension gradients are taking the lead after a spreading phase of about 60 s. As a result of these surface-tension gradients, topography measurement presents a steeper framing effect for a formulation with no surface agent closer to the substrate edge than for 0.3% or 0.6% surface agent formulations. Surface additives can avoid local surface-tension gradients and prevent the levelling flows, as shown by deflectometry measurement for 0.3% surface agent formulations.

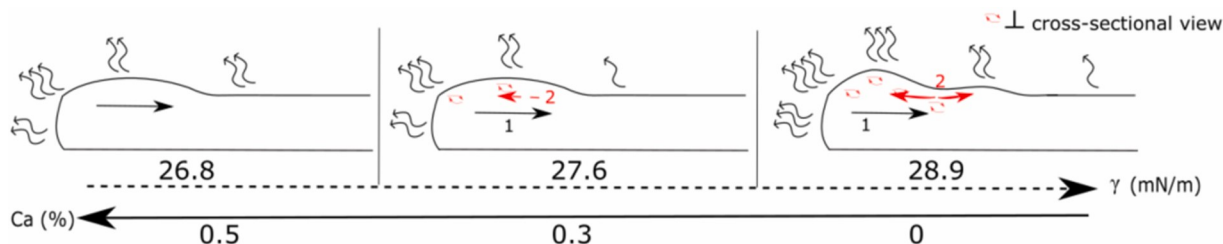


Fig. 13. Qualitative scheme presenting the influence of surface tension on coatings flows.

5. Conclusion

An innovative PTV technique applied to evaporative coatings allows flow analyses after film application and during evaporation. Different coating formulations were prepared with different surface-tension additive concentrations, and analyses of coating flow exhibited different behaviours for different coating formulations. All coating formulations experience a first spreading phase due to hydrostatic Laplace pressure.

Coating without or with a low amount of surface-tension additive exhibited lateral surface-tension gradients similar to levelling process, whereas coating with a surface-tension concentration above 0.3% did not indicate such movements. Correlation of these flows was possible with framing effect dynamics and final topography, coating without or with a low amount of surface-tension additive resulted in a steeper framing effect, which was narrower and closer to the substrate edge than coating with a higher amount of surface-tension additive. Considering the ability of surface tension additive to affect mass transfer through air-liquid interphase, we can conclude that the evaporation process leads to the framing effect dynamics. This paper has shown that coating formulation has a huge role in controlling framing effect: surface-tension additives present even at small concentration has the ability to modify drastically framing effect topography. This study has highlighted surface-tension gradients similar to levelling process [20] arising during film formation for the first time in an experimental work. Coating framing effect is a major defect in coating industry especially in decorative coatings and its topography has an influence on the visual perception of this defect and the material visual appearance. The influence of surface tension additives on other coating surface defects such as orange peel was, however, not included in this work.

Acknowledgements

We would like to thank C. Viera and Y. Wolters respectively for fruitful discussions and for supplying the paint material.

References

- [1] L. Weh, *Plaste Kautsch.* (1973) 138–141.
- [2] H. Hare, *C. Anat. Paint* (1992).
- [3] L.O. Kornum, Raaschou Nielsen, H. K. Surface defects in drying paint films, *Prog. Org. Coat.* (1980) 275–324.
- [4] O. Sommer, G. Wozniak, Investigation of coating liquid layer behaviour at curved solid edges, *Appl. Mech. Mater.* 831 (2016) 126–143.
- [5] Sommer, O. A contribution to the investigation of thin liquid layer behaviour at curved solid edges. (2014).
- [6] O. Sommer, S. Hehemann, G. Wozniak, Investigation of the behaviour of a Newtonian liquid regarding the picture framing coating error, e201800069, *PAMM* 18 (2018). e201800069.
- [7] A. Abbasian, S.R. Ghaffarian, N. Mohammadi, M.R. Khosroshahi, M. Fathollahi, Study on different planforms of paint's solvents and the effect of surfactants (on them), *Prog. Org. Coat.* 49 (2004) 229–235.
- [8] J.R.A. Pearson, *J. Fluid Mech.* 489 (1958).
- [9] N. Saranjam, S. Chandra, LU majeur - Bubble growth and movement in drying paint films, *Chem. Eng. Sci.* 145 (2016) 149–161.
- [10] G. Vazquez, G. Antorrena, J.M. Navaza, Influence of Surfactant Concentration and Chain Length on the Absorption of CO₂ by Aqueous Surfactant Solutions in the Presence and Absence of Induced Marangoni Effect, *Ind. Eng. Chem. Res* 39 (2000) 1088–1094.
- [11] L.K. Mudge, W.J. Heideger, The Effect of Surface Active Agents on Liquid-Liquid Mass Transfer Rates, *AIChE* (1970) 602–608.
- [12] J.T. Davies, *Turbulence Phenomena at Free Surface*, *AIChE* (1972) 169–173.
- [13] D.W. Thompson, Effect of Interfacial Mobility on Mass Transfer in Gas-Liquid Systems, *Ind. Eng. Chem. Fundam.* (1970) 243–248.
- [14] J.C. Burnett, D.M. Himmelbleau, The effect of surface active agents on interphase mass transfer, *AIChE* (1970) 185–193.
- [15] G. Lee, N. Hur, G. Son, A numerical analysis on the behavior of liquid film around a curved edge, *J. Comput. Fluids Eng.* 17 (2012) 75–80.
- [16] D.E. Weidner, L.W. Schwartz, R.R. Eley, Role of surface tension gradients in correcting coating defects in corners, *J. Colloid Interface Sci.* 179 (1996) 66–75.
- [17] M.H. Eres, D.E. Weidner, L.W. Schwartz, Three-dimensional direct numerical simulation of surface-tension-gradient effects on the leveling of an evaporating multicomponent fluid, *Langmuir* 15 (1999) 1859–1871.
- [18] L.W. Schwartz, D.E. Weidner, Modeling of coating flows on curved surfaces, *J. Eng. Math. - ematics* (1995) 91–103.
- [19] L.W. Schwartz, D.E. Weidner, R.R. Eley, An analysis of the effect of surfactant on the leveling behavior of a thin liquid coating layer, *Langmuir* (1995) 3690–3693.
- [20] S.E. Orchard, On surface levelling in viscous liquids and gels, *Appl. Sci. Res.* 11 (1963) 451–464.
- [21] S.K. Wilson, The levelling of paint films, *IMA J. Appl. Math.* 50 (1993) 149–166.
- [22] X. Wang, Y. Huang, C.E. Weinell, S.M. Olsen, S. Kiil, Leveling kinetics of coatings with solvent evaporation and non-Newtonian rheology, *Prog. Org. Coat.* 132 (2019) 169–177.

- [23] X. Wang, C.E. Weinell, V. Tobar, S.M. Olsen, S. Kiil, Leveling measurements of antifouling coatings using an optical profilometer: Effects of additives and solvent concentration and type, *Prog. Org. Coat.* 132 (2019) 159–168.
- [24] W.S. Overdiep, The levelling of paints, *Prog. Org. Coat.* 14 (1986) 159–175.
- [25] J. Roir'e, *Les. solvants* (1989).
- [26] ANOM (<https://www.digitalsurf.com/software-solutions/profilometry/>)
- [27] D. Karsa, *Surfactants in polymers, Coat., inks Adhes.* vol. 1 (2003).
- [28] H.J. Palmer, The hydrodynamic stability of rapidly evaporating liquids at reduced
- [29] T. Wei, F. Duan, Interfacial stability and self-similar rupture of evaporating liquid layers under vapor recoil, *Phys. Fluids* 28 (2016), 124106.
- [30] J. Zhang, R.P. Behringer, A. Oron, Marangoni convection in binary mixtures, *Phys. pressure, J. Fluid Mech.* 75 (1976) 487. *Rev. E* 76 (2007), 016306.